ORIGINAL RESEARCH

Toxicity-based toxicokinetic/toxicodynamic assessment of bioaccumulation and nanotoxicity of zerovalent iron nanoparticles in *Caenorhabditis elegans*

Ying-Fei Yang
Yi-Jun Lin
Chung-Min Liao

Department of Bioenvironmental Systems Engineering, College of Bioresources and Agriculture, National Taiwan University, Taipei, Taiwan

Abstract: Elucidating the relationships between the toxicity-based-toxicokinetic (TBTK)/toxicodynamic (TD) properties of engineered nanomaterials and their nanotoxicity is crucial for human health-risk analysis. Zerovalent iron (Fe^0) nanoparticles (NPs) are one of the most prominent NPs applied in remediating contaminated soils and groundwater. However, there are concerns that Fe^0NP application contributes to long-term environmental and human health impacts. The nematode *Caenorhabditis elegans* is a surrogate in vivo model that has been successfully applied to assess the potential nanotoxicity of these nanomaterials. Here we present a TBTK/TD approach to appraise bioaccumulation and nanotoxicity of Fe^0NPs in *C. elegans*. Built on a present *C. elegans* bioassay with estimated TBTK/TD parameters, we found that average bioconcentration factors in *C. elegans* exposed to waterborne and food-borne Fe^0NPs were ~50 and ~5×10^{-3}, respectively, whereas 10% inhibition concentrations for fertility, locomotion, and development, were 1.26 (95% CI 0.19–5.2), 3.84 (0.38–42), and 6.78 (2.58–21) $\mu g \cdot g^{-1}$, respectively, implicating that fertility is the most sensitive endpoint in *C. elegans*. Our results also showed that biomagnification effects were not observed in waterborne or food-borne Fe^0NP-exposed worms. We suggest that the TBTK/TD assessment for predicting NP-induced toxicity at different concentrations and conditions in *C. elegans* could enable rapid selection of nanomaterials that are more likely to be nontoxic in larger animals. We conclude that the use of the TBTK/TD scheme manipulating *C. elegans* could be used for rapid evaluation of in vivo toxicity of NPs or for drug screening in the field of nanomedicine.

Keywords: zerovalent iron nanoparticles, *Caenorhabditis elegans*, nanotoxicology, bioaccumulation, toxicity-based-toxicokinetic/toxicodynamic modeling

Introduction

In the fields of environmental nanotechnology, zerovalent iron (Fe^0) nanoparticles (NPs) are one of the most prominent NPs applied in remediating contaminated soils and groundwater. However, despite the low cost and high efficiency of Fe^0NPs in removing contaminants,[1–6] there are concerns that Fe^0NP application contributes to long-term impacts on environmental and human health risks.[7–17] Moreover, the increasing use of Fe^0NPs in in situ groundwater remediation could lead to large numbers of NPs released into the environment and is highly likely to pose potential exposure risks.[8]

Several studies have indicated that Fe^0NPs could cause cytotoxicity in human bronchial epithelial cells.[8,18,19] Previous studies on the effects of Fe^0NPs on microorganisms, such as *Bacillus cereus*, *Pseudomonas stutzeri*, and *Escherichia coli*, have

Correspondence: Chung-Min Liao
Department of Bioenvironmental Systems Engineering, College of Bio-Resources and Agriculture, National Taiwan University, 1 Roosevelt Road, Section 4, Taipei 10617, Taiwan
Tel +886 2 2363 4512
Email cmliao@ntu.edu.tw

revealed that Fe might be reduced from NPs to lead to stress responses.[7,17,20] Inhibition in embryo development, mortality of spermatozoa, and declines in fertilization in embryos were observed in marine microalgae in response to Fe^0NP exposure.[12] Li et al[21] indicated that FeNPs disturbed defense systems in embryos of medaka fish. Chen et al[14] further found that Fe^0NPs had significant adverse effects on heart rates and eye sizes in early stages of medaka fish.

Although the nanotoxicological knowledge of Fe^0NPs is growing,[22–25] toxicity-based-toxicokinetic (TBTK)/toxicodynamic (TD) assessments describing the fate and behavior of Fe^0NPs in living organisms are not well understood and remain a substantial challenge. TBTK/TD modeling is a robust mechanistic approach enabling integration of toxic effects on multiple endpoints over time.[26–28] Toxicokinetics deal with the time course encompassing absorption, distribution, biotransformation, and elimination of toxicants by linking external exposure concentrations to biologically effective doses, whereas toxicodynamics describe processes leading from toxic actions to subsequent impairments in organisms. Therefore, TBTK/TD modeling provides a rigorously quantitative framework to understand the diverse nanotoxicological issues better.

Although most parameters of pharmacokinetics, biodistribution, and efficacy are typically assessed in mice,[29] a larger number of smaller organisms could potentially be used to obtain the physiological effects of NPs on animal development.[30] The invertebrate *Caenorhabditis elegans* is a species of soil-dwelling nematode (roundworm) used as a model organism in molecular genetics and developmental biology. It is predominantly hermaphroditic (can self-fertilize), transparent, and effective in assessing environmental and human health risks.[31–33] Moreover, *C. elegans* is a well-known model and has recently been used to assess the effects of various types of nanomaterials and the pharmacological and in vivo toxic effects of drugs, implicating their importance in the field of nanomedicine.[30,34,35]

There is limited information on TBTK/TD-based assessments for metal-based NP-contaminated *C. elegans*. However, several TBTK/TD modeling studies related to the relationships between the potential nanotoxicity of specific contaminants in *C. elegans* and their associated environments may provide proper methods for predicting the toxicity of nanomaterials. The mixed-toxicity effects of Cd and fluoranthene in *C. elegans* have been interpreted using an energy-based TBTK/TD model.[36] A two-compartmental TBTK modeling of phenanthrene in *C. elegans* has been performed,[37] indicating that waterborne exposure was the major route to bioaccumulated compound in the nematode tissues. A recent study also employed a TBTK/TD energy-based model to describe the joint toxicity of uranium and Cd over growth and reproduction periods in *C. elegans*.[38]

Given that, to the best of our knowledge, no single study to date has assessed the nanotoxicity response of Fe^0NPs associated with *C. elegans* in an in vivo model, a challenge exists in how to integrate TBTK/TD information and a risk-assessment framework reliably to derive predictable risk trends. Therefore, results obtained with this surrogate model are critical to provide new approaches in nanotoxicology and to predict their toxic effects in living organisms. Accordingly, the purpose of this study was to evaluate Fe^0NP body burden over time in *C. elegans* and their food sources *E. coli*, whereas to obtain the dose–response relationships based on the TD model among different endpoints. A metal NP-based TBTK/TD model with adequate predictive power can be used to guide experimental designs and to reduce animal testing and costs. Most importantly, the TBTK/TD modeling is capable of simulating and predicting bioaccumulation levels in living organisms and their response to metal NPs.

Materials and methods
Fe^0NP characterization

Fe^0NPs were synthesized by the borohydride-reduction approach in the presence of carboxymethyl cellulose (molecular weight 90,000 Da), as previously described.[39] To analyze size distribution of Fe^0NPs, freshly prepared Fe^0NPs were sonicated for 30 minutes before being analyzed by dynamic light scattering (Delsa Nano C; Beckman Coulter, Brea, CA, USA). Morphological features of Fe^0NPs were analyzed by transmission electron microscopy (JEM1200EXII; JEOL, Tokyo, Japan). Dynamic elements of Fe^0NPs, such as pH, dissolved oxygen, oxidation-reduction potential, and iron speciation, have been described in a previous study.[10] To analyze the dynamic size distribution of Fe^0NPs in the presence of *E. coli* OP50, Fe^0NP samples were collected time-dependently and analyzed immediately by dynamic light scattering.

Bioaccumulation experiment

Synchronized L1 larvae of *C. elegans* were exposed to waterborne or food-borne 100 $mg·L^{-1}$ Fe^0NPs in the medaka embryo-rearing medium (ERM) supplemented with Fe^0NP-unexposed or Fe^0NP-exposed *E. coli* OP50 (optical density [OD] =1.1) for 5 days of uptake and transferred to clean nematode-growth medium (NGM) agar plates for 2 days of depuration. Two treatments of waterborne and food-borne Fe^0NP

exposures were conducted. Test flasks for the treatment of waterborne Fe⁰NPs contained 50 mL of ERM supplemented with clean *E. coli* OP50 as a food source with 100 mg·L⁻¹ Fe⁰NPs. For food-borne Fe⁰NP treatment, test flasks contained 50 mL of ERM including Fe⁰NP-exposed *E. coli* OP50. Flasks were kept in the dark at 20°C. Samples of bacteria, worms, and suspension medium were collected at various time points, from the day organisms were exposed to Fe⁰NPs to the day they were transferred to clean NGM plates.

In waterborne and food-borne Fe⁰NP treatments, bacteria contained in medium were centrifuged to collect bacteria pellets at 14,000 rpm for 5 minutes. Pellets of bacteria were heated at 60°C overnight, then acidified with 0.1 N HCl for subsequent measurement of total iron concentrations in both Fe⁰NP-unexposed and Fe⁰NP-exposed bacteria pellets. Aqueous iron concentrations in the medium were also determined by acidifying suspension of samples with 0.1 N HCl after centrifugation for further measurements of total iron concentrations. To determine internal iron concentrations of worms, at least 5,000 worms were collected in each time series. There was no discrimination in worm collection between parental and filial generation after 72 hours in the exposure period. Subsequently, samples were homogenized by sonication and acidified with 0.1 N HCl for measurements of total iron concentrations. Total biomass of worms was calculated by multiplying the mean weight of 4.2 µg per worm.[40,41]

Ecotoxicity bioassays

Three kinds of bioassay were conducted to observe the nanotoxicity of Fe⁰NPs in *C. elegans*: fertility, locomotion, and development. Data of infertility effects posed by Fe⁰NPs were adopted from a previous study,[42] with new data entries based on the present fertility bioassay. The fertility bioassay was adopted mainly from a previous study.[43] Briefly, synchronized wild-type L4 larvae were exposed to concentrations of 5, 25, 50, 100, 250, and 500 mg·L⁻¹ of Fe⁰NPs for 48 hours in the presence of *E. coli* OP50 (OD =0.4) at 20°C. Subsequently, the offspring of each nematode were scored.

On the other hand, for bioassays of locomotion and development, synchronized wild-type L1 larvae were exposed to concentrations of 5, 25, 50, 100, 250, and 500 mg·L⁻¹ Fe⁰NPs for 65 hours in the presence of *E. coli* OP50 (OD =1.1) at 20°C. Before analysis of locomotive behaviors and development, worms were washed with double-distilled water three times to remove adherent bacteria and transferred to NGM plates to observe their locomotion and development. The bioassay of locomotive behaviors was performed by counting body bends of worms,

adapted from a previous study.[44] After a recovery period of 1 minute on NGM plates, the body bends of worms were counted at intervals of 20 seconds. A body bend was counted as a change in direction of the part of worm corresponding to the posterior bulb of pharynx along the *y*-axis, with the assumption that the worm was traveling along the *x*-axis.

For the development bioassay, randomly selected worms from each treatment were mounted onto microscope slides coated with 1% agarose, anesthetized with 1 mM sodium azide, and capped with coverslips. Body length was captured with epifluorescence microscopy (Leica, Wetzlar, Germany) and a cooled charge-coupled-device camera. The body length of each individual worm was analyzed by ImageJ software. Approximately 20 worms were examined per treatment. At least three biological experiments were repeated.

Chemical analysis

Samples of worms, bacteria, and supernatant in various time series were frozen with liquid nitrogen immediately before being analyzed for total iron concentration. To examine internal iron concentrations, worms were washed three times with deionized water to discard Fe⁰NPs in the exposing medium and cuticles of worms. Subsequently, worms were homogenized by sonication and acidified with 0.1 N HCl. To determine bioaccumulation of Fe⁰NPs in *E. coli* OP50, pellets of bacteria were washed with deionized water three times to eliminate adherent iron on cell membranes and recollected by centrifugation (14,000 rpm, 5 minutes). Pellets of bacteria were then dried for 6 hours at 55°C to eliminate residual double-distilled H₂O in bacteria pellets, weighted to determine dry weight, and acidified with 0.1 N HCl overnight for subsequent analyses of internal iron concentrations.

For total iron concentrations in supernatants of Fe⁰NP dosing medium, since Fe⁰NPs had settled quickly due to particle agglomeration and aggregation, a dosing solution of 100 mg·L⁻¹ Fe⁰NPs was digested overnight with 0.1 N HCl for subsequent measurement. Internal concentrations in worms and bacteria along with actual exposure concentrations in medium were determined colorimetrically by the ferrozine method.[45]

Biodynamics of Fe⁰NP-*E. coli*–*C. elegans* interactions (TBTK modeling)

A first-order two-compartment model was developed to predict Fe⁰NP concentrations in worms and bacteria. The biodynamics of Fe⁰NP-*E. coli*–*C. elegans* interactions (Figure 1A) were constructed: 1) the exchange of Fe⁰NPs (or other Fe forms) between worms and Fe⁰NPs was
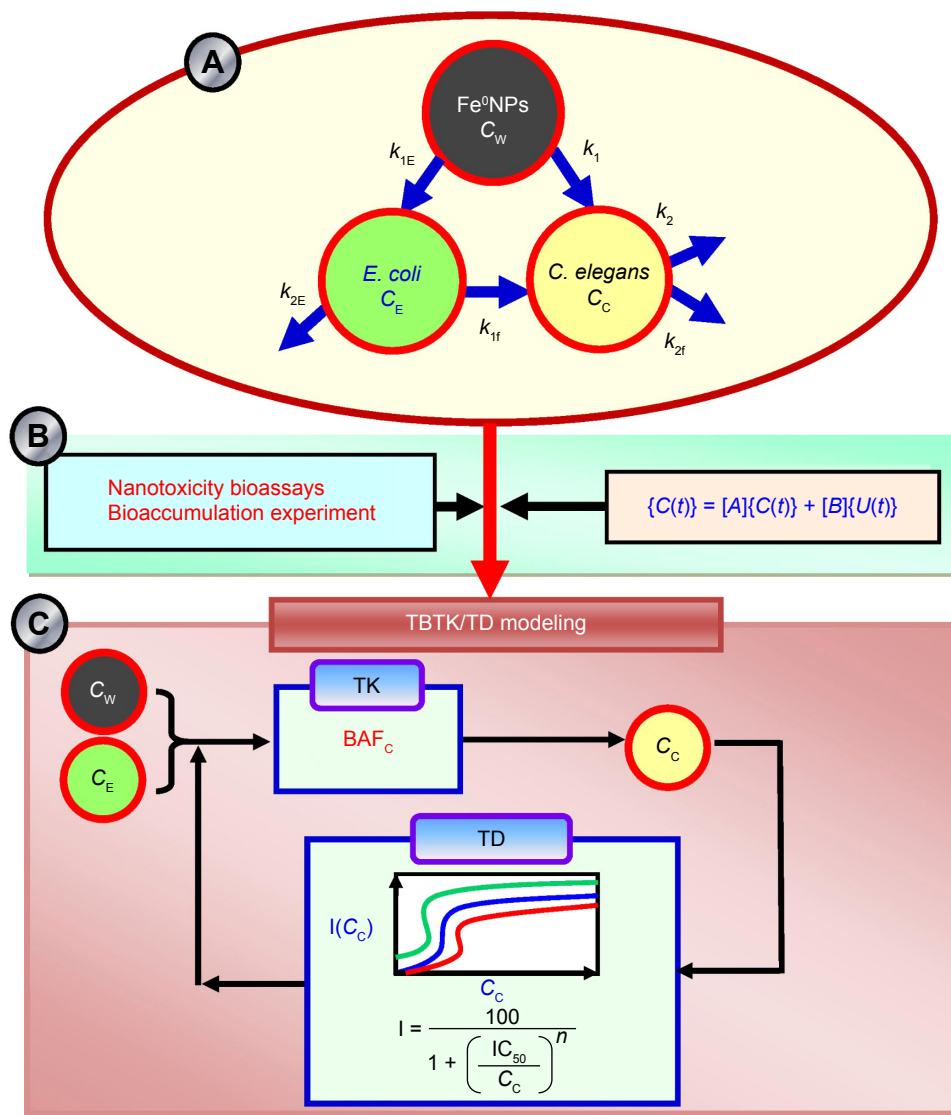
Figure 1 Framework of TBTK/TD ecological risk assessment of Fe⁰NPs for *Caenorhabditis elegans* in soil ecosystems.

Notes: (**A**) Biodynamics of Fe⁰NP *Escherichia coli*–*C. elegans* interactions; (**B**) development of first-order two-compartment models and bioassays based on the constructed biodynamic system; (**C**) TBTK/TD modeling.

Abbreviations: TBTK, toxicity-based-toxicokinetic; TD, toxicodynamic; NPs, nanoparticles; *C*, constant Fe⁰NP concentrations; E, *E. coli* OP50; C, *C. elegans*; W, waterborne; k_1, uptake-rate constant; k_2, depuration-rate constant; f, food-borne; *C(t)*, time-dependent Fe⁰NP concentrations; BAF$_c$, bioaccumulation factor; *I*, inhibition; IC$_{50}$, 50% inhibition concentration.

modeled as a first-order process, with additional Fe⁰NPs (or other Fe forms) accumulated from ingested bacteria (food-borne route); 2) body burden of Fe⁰NPs (or other Fe forms) per unit biomass of worms increases as a result of direct uptake from water (waterborne route) and through assimilation of Fe⁰NP-contaminated bacteria (food-borne route); 3) body burden of Fe⁰NPs (or other Fe forms) tends to decrease as a result of elimination from the whole body of worms; and 4) growth dilution of worms was negligible in the model.

The first-order two-compartment model for gain and loss of Fe⁰NPs accumulation in worms and bacteria features constant biokinetic reaction rates and water concentration. Specifically,

the underlying biodynamics of Fe⁰NP-*E. coli*–*C. elegans* interactions (Figure 1A and B) are governed by a set of ordinary differential equations (Equations 1 and 2, Table 1) where *t* is the time of exposure (h), $C_E(t)$ (µg·g⁻¹ wet weight) the time-dependent Fe⁰NP concentrations in bacteria, C_w the constant Fe⁰NP concentration in water (µg·mL⁻¹), k_{1E} the uptake-rate constant from Fe⁰NPs by bacteria (mL·g⁻¹·h⁻¹), k_{2E} the depuration-rate constant from Fe⁰NPs by bacteria (h⁻¹), $C_c(t)$ the time-dependent Fe⁰NP concentrations in worms (µg·g⁻¹ wet weight), k_1 the uptake-rate constant from waterborne Fe⁰NPs by worms (mL·g⁻¹·h⁻¹), k_2 the depuration-rate constant from waterborne Fe⁰NPs by worms (h⁻¹), k_{1f} the uptake-rate constant from food-borne Fe⁰NPs by worms

Table 1 Equations for TBTK/TD modeling and risk model used in this study

TBTK model

$$\frac{dC_E(t)}{dt} = k_{1E}C_W - (k_{2E} + k_{1f})C_E(t) \tag{1}$$

$$\frac{dC_C(t)}{dt} = k_1 C_W + k_{1f}C_E(t) - (k_2 + k_{2f})C_C(t) \tag{2}$$

$$C_E = \left(\frac{k_{1E}}{k_{2E} + k_{1f}}\right) \times C_W = BCF_E \times C_W \tag{3}$$

$$C_C(t) = C_{C,0}e^{-k_e t} + \frac{k_u}{k_e}C_W(1 - e^{-k_e t}) \tag{4}$$

$$C_C = \frac{k_u}{k_e}C_W = BAF_C \times C_W \tag{5}$$

$$BAF_C = \frac{k_u}{k_e} = \frac{BCF_{C_W}}{1 + k_{2f}k_2^{-1}} + BMF_{Cf} \times BCF_E \tag{6}$$

TD model

$$I(C) = \frac{I_{max}}{1 + \left(\dfrac{IC_{50}}{C}\right)^n} \tag{7}$$

$$I(C_C) = \frac{I_{max}}{1 + \left(\dfrac{C_{I,50}}{C_C}\right)^n} \tag{8}$$

$$P(I|C_C) = \Phi\left(\frac{I_{max}}{1 + \left(\dfrac{C_{I,50}}{C_C}\right)^n}\right) \tag{9}$$

Predictive risk threshold model

$$F(C_C) = 1 - \exp\left[-\left(\frac{C_C - \gamma}{\alpha}\right)^\beta\right], C_C > \gamma > 0, \alpha > 0, \beta > 0 \tag{10}$$

Abbreviations: TBTK, toxicity-based-toxicokinetic; TD, toxicodynamic; $C(t)$, time-dependent Fe⁰NP concentrations; C, constant Fe⁰NP concentrations; $C_{C,0}$, initial Fe⁰NP concentration in worms; E, *E. coli* OP50; C, *C. elegans*; k_1, uptake-rate constant; k_2, depuration-rate constant; w, waterborne Fe⁰NPs; f, food-borne Fe⁰NPs; BCF, bioconcentration factor; BAF, bioaccumulation factor; BMF, biomagnification factor; *I*, inhibition; *P*, probability; Φ, cumulative density function; F(C_C), cumulative density function data; α, scale parameter; β, shape parameter, γ, threshold.

$(g \cdot g^{-1} \cdot h^{-1})$, and k_{2f} the depuration-rate constant from food-borne Fe⁰NPs by worms (h^{-1}).

To simplify the biodynamic behavior, we reasonably assume Fe⁰NP body burden in bacteria undergoes a steady-state process. This assumption is a somewhat crude simplification, yet sufficient to explore the overall impact of Fe⁰NPs on biodynamics. We can then solve the steady-state Fe⁰NP body burden in bacteria given by Equation 3 (Table 1) where BCF_E is the bioconcentration factor for Fe⁰NPs in bacteria $(mL \cdot g^{-1})$. Therefore, $C_C(t)$ can be solved directly by substituting Equation 3 into Equation 1 as Equation 4 (Table 1), where $k_u = k_1 + k_{1f}BCF_E$, $k_e = k_2 + k_{2f}$, and $C_{C,0}$ is the initial Fe⁰NP concentration at $t=0$ $(\mu g \cdot g^{-1}$ wet weight) in worms.

Finally, the steady-state condition for Fe⁰NP bioaccumulation in worms was solved as Equation 5 (Table 1), where BAF_C is the bioaccumulation factor for Fe⁰NPs in worms $(mL \cdot g^{-1})$ and can be mathematically expressed as Equation 6 (Table 1), where BCF_{Cw} is the bioconcentration factor for waterborne Fe⁰NPs in worms $(mL \cdot g^{-1})$ and BMF_{Cf} the biomagnification factor for food-borne Fe⁰NPs in worms $(g \cdot g^{-1})$. The input variables needed to model Fe⁰NP bioaccumulation in bacteria and worms include biokinetic parameters (k_{1E}, k_{2E}, k_1, k_2, BCF_{Cw}, and BMF_{Cf}) and the geochemical variable of C_w.

Dose–response-based TD modeling

We constructed the concentration–response relationships for inhibition of fertility, locomotion, and development versus Fe⁰NP body burden in worms by fitting the three-parameter Hill model[46] to published[42] and present bioassay data sets. In fitting the Hill model to the observed endpoints, the dose–response profiles can be expressed as Equation 7 (Table 1) where $I(C)$ is the inhibition of fertility, locomotion, and development (%), respectively, to specific exposure concentrations of Fe⁰NPs – C $(mg \cdot L^{-1})$. In Equation 7, I_{max} is the maximum inhibition of fertility, locomotion, and development (%) to specific exposure concentrations of Fe⁰NPs, IC_{50} the concentration of Fe⁰NPs causing 50% inhibition of fertility, locomotion, and development $(mg \cdot L^{-1})$, and n the fitted Hill coefficient, such that $n=1$ represents a linear response fashioned as the Michaelis–Menton mode and $n>1$ represents a sigmoidal response that is ultrasensitive to the toxicants (Table 1).

To convert external concentration to internal body burden, Equation 7 can be used to transform to a body burden–response relationship expressed as Equation 8 (Table 1), where $C_{I,50}$ is the internal effect concentrations at the site of action that cause 50% inhibition of fertility, locomotion, and development, respectively. The IC_{50} data were adopted from the model fitted to Equation 8 probabilistically (Table 1). The IC_{50} cumulative distribution functions (CDFs) of predicted functions of inhibition of fertility, locomotion, and development for a given Fe⁰NP body burden, $P(I|C_C)$, were obtained by applying the Hill model, and can be expressed as a conditional probability function (Equation 9, Table 1), where C_c is the given Fe⁰NP body burden and Φ(•) the cumulative standard normal distribution (Figure 1C).

Predictive risk-threshold modeling

A three-parameter Weibull threshold model (Equation 10, Table 1) was employed to fit the IC_{50} toxicity data best to estimate threshold concentrations that can protect *C. elegans* from inhibition of fertility, locomotion, and development exposed to waterborne Fe⁰NPs. The toxicity data were

Table 2 k_1, k_2, BCF, and BMF values (mean ± SE) of bacteria *Escherichia coli* OP50 and worm *Caenorhabditis elegans* calculated from laboratory Fe⁰NP-exposure experiments

	Uptake phase		Depuration phase		
	k_1 (mL·g⁻¹·h⁻¹ [waterborne], g·g⁻¹·h⁻¹ [food-borne])	k_2 (h⁻¹)	k_2 (h⁻¹)	BCF	BMF
Bacteria	0.829±0.52 (k_{1E})	0.01±0.018 (k_{2E})	0.07±0.039	82.9 (BCF$_E$)	
Worms	0.046±0.034 (k_1)	0.001±0.015 (k_2)	0.07±0.064	46 (BCF$_{Cw}$)	0.55 (BMF$_{Cw}$)
Water-exposed					
Food-exposed	(0.082×10⁻³) ± (0.034×10⁻³) (k_{1f})	0.016±0.013 (k_{2f})	0.011±0.002	0.005 (BCF$_{Cf}$)	6.03×10⁻⁵ (BMF$_{Cf}$)

Abbreviations: SE, standard error; NP, nanoparticle; k_1, uptake-rate constant; k_2, depuration-rate constant; E, *E. coli* OP50; C, *C. elegans*; w, waterborne Fe⁰NPs; f, food-borne Fe⁰NPs; BCF, bioconcentration factor; BAF, bioaccumulation factor; BMF, biomagnification factor.

obtained from estimated IC_{50} CDFs (Equation 9, Table 1). In Equation 10, $F(C_c)$ represents the IC_{50} CDF data corresponding to specific Fe⁰NP body burden in worms, α the scale parameter that affects the distribution as a change of the abscissa scale, β the shape parameter representing the slope of the line in the CDF, and γ the fitted threshold (µg·g⁻¹). The Weibull threshold model was used to fit to extracted percentiles 2.5, 5, 50, 95, and 97.5 of IC_{50} CDF data.

Uncertainty and sensitivity analyses

Table Curve 2D (version 5.01; AISN Software, Mapleton, OR, US) was used to perform all model fittings. A Monte Carlo analysis was incorporated to obtain percentiles 2.5 and 97.5 as the 95% CI for all uncertainty analyses. Parameterization and sensitivity analysis of variables were performed by using 10,000 Monte Carlo simulations. The Monte Carlo simulation was implemented using Crystal Ball software (version 2000.2; Decisioneering, Denver, CO, USA).

Results and discussion
TBTK analysis in bacteria

To obtain TBTK-parameter estimates of k_{1E} and k_{2E} for bacteria, the first-order kinetic model (Equation 1) was used to fit the exposure data (Table S1; Table 2; Figure 2A and B). The estimated Fe⁰NP body burden in bacteria at the steady state (C_E) was 2,167.95±1,445.84 µg·g⁻¹ (mean ± SD) (Table S2). Although the bactericidal effects of Fe⁰NPs have been reported in several studies,[3,7,20] factors causing the lethal effects to bacteria are dependent on species of bacteria, physiochemical characteristics, and concentrations of Fe⁰NPs. Previous research has indicated that 70–700 mg·L⁻¹ Fe⁰NPs are likely to cause bactericidal effects on *E. coli* Qc1301.[7] However, our study did not observe 100 mg·L⁻¹ Fe⁰NPs causing lethal effects in *E. coli* OP50, due in part to the differences in bacterial species and chemical properties of Fe⁰NPs. Our result is supported by a previous study,[3] indicating a lack of toxicity of Fe⁰NPs on the Gram-negative strain of *Klebsiella planticola*. It was

also found that Fe⁰NPs had no effect on bacterial populations when Fe⁰NPs were coated with biodegradable organic compounds,[47] supporting a lower bactericidal effect of carboxymethyl cellulose-coated Fe⁰NPs observed in this study.

It has been found that *E. coli* has no endocytic function for uptake of NPs.[48] Plausible mechanisms that regulate internalization of NPs into bacteria may include nonspecific diffusion, damage to bacterial cell membranes by release of metal ions, and gene-transport systems.[49–51] Studies
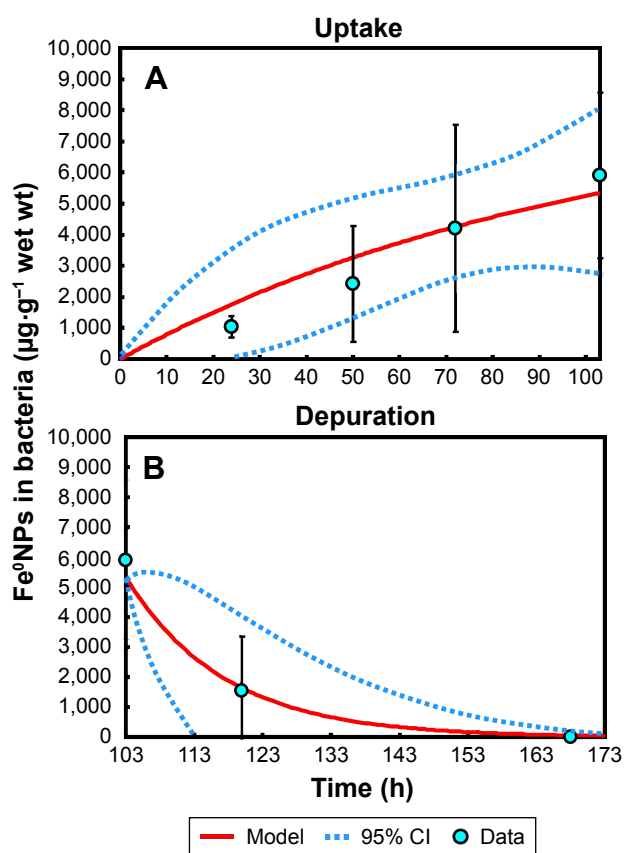

Figure 2 Toxicokinetics of (**A**) uptake and (**B**) depuration of Fe⁰NPs by the bacteria *Escherichia coli* OP50 during 103 hours' exposure and then 65 hours' depuration.
Notes: Solid circles are measurements of Fe⁰NP body burdens in bacteria. Solid and dotted lines are model simulations and 95% CIs of original data points, respectively.
Abbreviations: NP, nanoparticle; wt, weight; h, hour; CI, confidence interval.

have also shown evidence that NPs can be taken up by bacteria at nonbactericidal doses by interacting with macromolecules of cell membranes or by disrupting membrane integrity.[7,49] Therefore, Fe⁰NPs could be accumulated in bacteria through internalization of NPs or be adhered on cell membranes of bacteria with Fe oxides.[52]

TBTK analysis in worms

To observe internal Fe⁰NPs in worms at the steady state without being unable to distinguish between parental and filial generations, we performed a TBTK experiment for 5 days in the uptake phase. The filial generation was fertilized after 72 hours in the uptake phase, and the progeny consumed Fe⁰NPs and food with parental generation at the same time. However, worms were kept from starvation and overcrowded during exposure. In our TBTK experiments, although Fe⁰NPs are easily oxidized to Fe-oxides and Fe ions under aerated

conditions, total Fe remained stable during the exposure.[10] In addition, our estimated Fe⁰NP body burdens in worms were all above the detection limit of $0.5 \ \mu g \cdot L^{-1}$.[53]

Based on the first-order kinetic model (Equation 2), uptake- and elimination-rate constants between waterborne Fe⁰NPs and worms (k_1 and k_2, respectively) and rates between food-borne Fe⁰NPs and worms of k_{1f} and k_{2f} were obtained (Table 2; Figure 3). While our estimates of uptake parameters (k_1 and k_{1f}) were much smaller than worms exposed to organic compounds, the elimination-parameter estimates (k_2 and k_{2f}), however, were consistent with those of a previous study (Table 2).[31] Similar to results of other TBTK studies,[54,55] elimination parameters were relatively dependent on organisms. Factors causing differences in estimates of uptake parameters are strongly associated with different mechanisms in the bioaccumulation of chemicals. Nevertheless, metal-based NPs depend on surrounding medium and chemical forms,
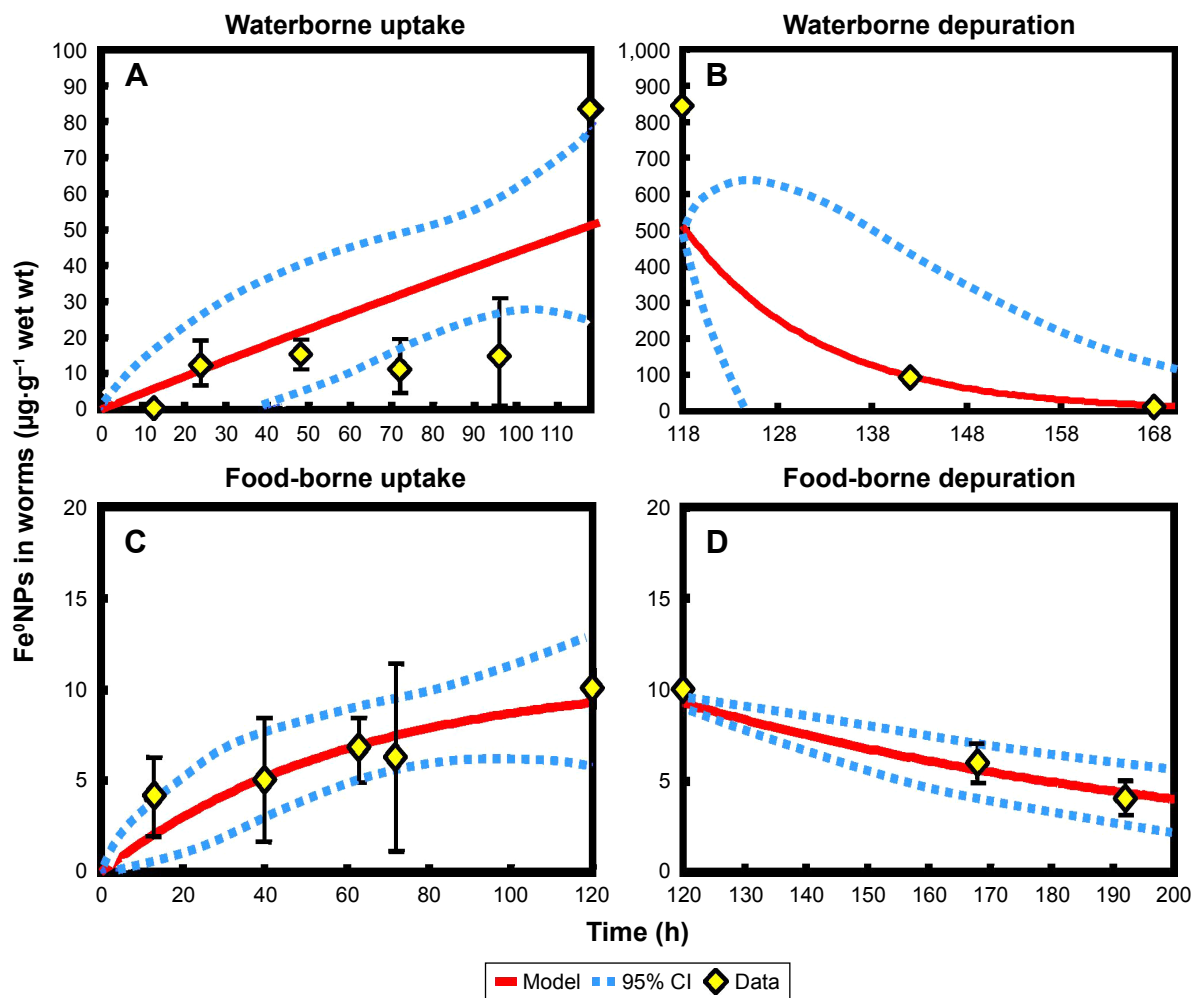

Figure 3 Uptake and depuration of (**A**, **B**) water-exposed and (**C**, **D**) food-exposed Fe⁰NPs by the worm *Caenorhabditis elegans*.
Notes: During 118 and 120 hours' exposure and then 50- and 72-hour depuration periods. Solid diamonds are measurements of Fe⁰NP body burdens in worms. Solid and dotted lines are model simulations and 95% CIs of original data points, respectively.
Abbreviations: NP, nanoparticle; wt, weight; h, hour; CI, confidence interval.

whereas the organic substances depend on hydrophobicity and sorption sites.[56,57] It has been suggested that estimates of uptake parameters generally depend on exposure conditions and medium characteristics.[54] Fe⁰NPs can easily form aggregations in media with higher ionic strength and interact with bacteria, resulting in bioavailability reduction of Fe⁰NPs and alternation of uptake parameters in worms.

It was observed that BCF values in worms were smaller than in bacteria, supported by a previous study that body burdens of Cd in bacteria were higher in worms than in bacteria.[58] The trends of TBTK estimates were also consistent with a previous study where values of uptake parameters were higher than elimination ones (Table 2).[59] The uptake constants of waterborne Fe⁰NP-exposed worms were higher than those of food-borne-treated ones, suggesting that Fe⁰NPs accumulated easily in worms via waterborne routes (Table 2). We found that Fe⁰NP body burdens and BCFs were relatively low in worms, similar to results of other studies and BCFs of Fe⁰NPs in medaka fish.[10,59] The BMFs were smaller than 1 in both waterborne and food-borne Fe⁰NP-exposed worms (Table 2), indicating that biomagnification effects did not occur in the food-chain structure of *E. coli–C. elegans*. The biomagnification effects of various metal-based NPs, such as CdSe quantum dots, Au, CeO₂, and TiO₂, have been evidenced in several studies.[60–63] However, several NPs with conflicting results have been reported to have no biomagnification effects in food chains.[64–67] Tangaa et al[68] and Unrine et al[69] suggested that the discrepancies among BMFs could be due to both abiotic (eg, environmental parameters) and biotic (eg, organism physiology and life-history traits, food-web structure, and analyses of whole-body vs single-organ concentration) that affect the efficiency of trophic transfer.

Aqueous concentrations of Fe⁰NPs remained constant and averaged 58.86 mg·L⁻¹ in the treatment of waterborne Fe⁰NPs during the exposure period of 120 hours (Figure S1). However, concentrations in the treatment of food-borne Fe⁰NPs were 1.63–2.48 mg·L⁻¹ and decreased at ~90 hours during the exposure period (Figure S1), suggesting that Fe⁰NPs in the exposure media were able to be easily consumed by worms via assimilation of bacteria.

Probability distributions of TBTK parameters and BCFs in bacteria and worms

Overall, the trends of probability distributions of TBTK parameters and BCFs were in accordance with estimated results in Table 2. A lognormal (LN) probability model can best fit the experimental data of Fe⁰NP body burden in bacteria, resulting

in a geometric mean (GM) of 0.50 mL·g⁻¹·h⁻¹ and a geometric standard deviation (GSD) of 1.82 (LN[0.5 mL·g⁻¹·h⁻¹, 1.82]) in the uptake phase (Figure 4A), and LN(0.001 h⁻¹, 3.28) in the elimination phase (Figure 4B).

In the uptake phase of worms exposed to waterborne Fe⁰NPs, GMs of k_1 and k_2 were 0.02 mL g⁻¹·h⁻¹ and 1.02×10^{-6} h⁻¹ with GSDs of 1.93 and 5.74, respectively (Figure 4C and D). For worms exposed to food-borne Fe⁰NPs, GMs of k_{1f} and k_{2f} were 6.51×10^{-5} g·g⁻¹·h⁻¹ and 0.01 h⁻¹ with GSDs of 1.48 and 2.1, respectively (Figure 4E and F).

On the other hand, Figure 5A illustrates the best-fit probability distributions for BCF in bacteria with LN (108 mL·g⁻¹ wet weight, 5.16). The high GSD values of distributions of elimination-rate constants were attributed to the high SE values predicted in Table 2. Figure 5B and C illustrate the best-fit probability distributions for BCF in worms exposed to waterborne and food-borne Fe⁰NPs with LNs of 50.1 (4.17) and 7.32×10^{-3} (2.75), respectively. The GM values of uptake-rate constant and BCF in food-borne Fe⁰NP-exposed worms were much lower than waterborne-treated ones, probably due to the lower actual concentrations of Fe⁰NPs of the food-borne source.[70] Furthermore, Figure 5D shows the best-fit probability distributions for BAF in worms generated from probability distributions of BCF_E, BCF_{Cw}, and BCF_{Cf} (Figure 5A–C) with LN (0.034, 6). The BAF could be used for prediction of internal body burdens in worms with information of Fe⁰NP environmental concentrations.

TD analysis in worms

To avoid effects on reproduction, the possible interaction with Fe⁰NPs, and experimental parameters in worms (eg, pharyngeal pumping rates, body size, and morphology),[71–73] we did not use 5-fluoro-2′-deoxyuridine in our study. Also, to reflect a realistic scenario in soil ecosystems and to prevent possible effects on physiology in worms confounding TD of Fe⁰NPs,[74] we did not use infertile mutants for preventing progeny production, as in a previous study.[41]

The relationships between Fe⁰NP-exposure concentrations and inhibition of fertility, locomotion, and development (%) for worms can be well fitted to a Hill-based dose–response profile (Figure 6). Overall, the estimated Fe⁰NP-exposure concentrations causing IC₁₀ are in the order of development > locomotion > fertility, with estimates of 6.78 (95% CI 2.58–21), 3.84 (95% CI 0.38–42), and 1.26 (95% CI 0.19–5.2) μg·g⁻¹, respectively (Figure 6, Table S3). It was found that fertility was the most sensitive end point in *C. elegans* to Fe⁰NP toxicity. A previous study supported our results that both growth and fertility of *C. elegans* were
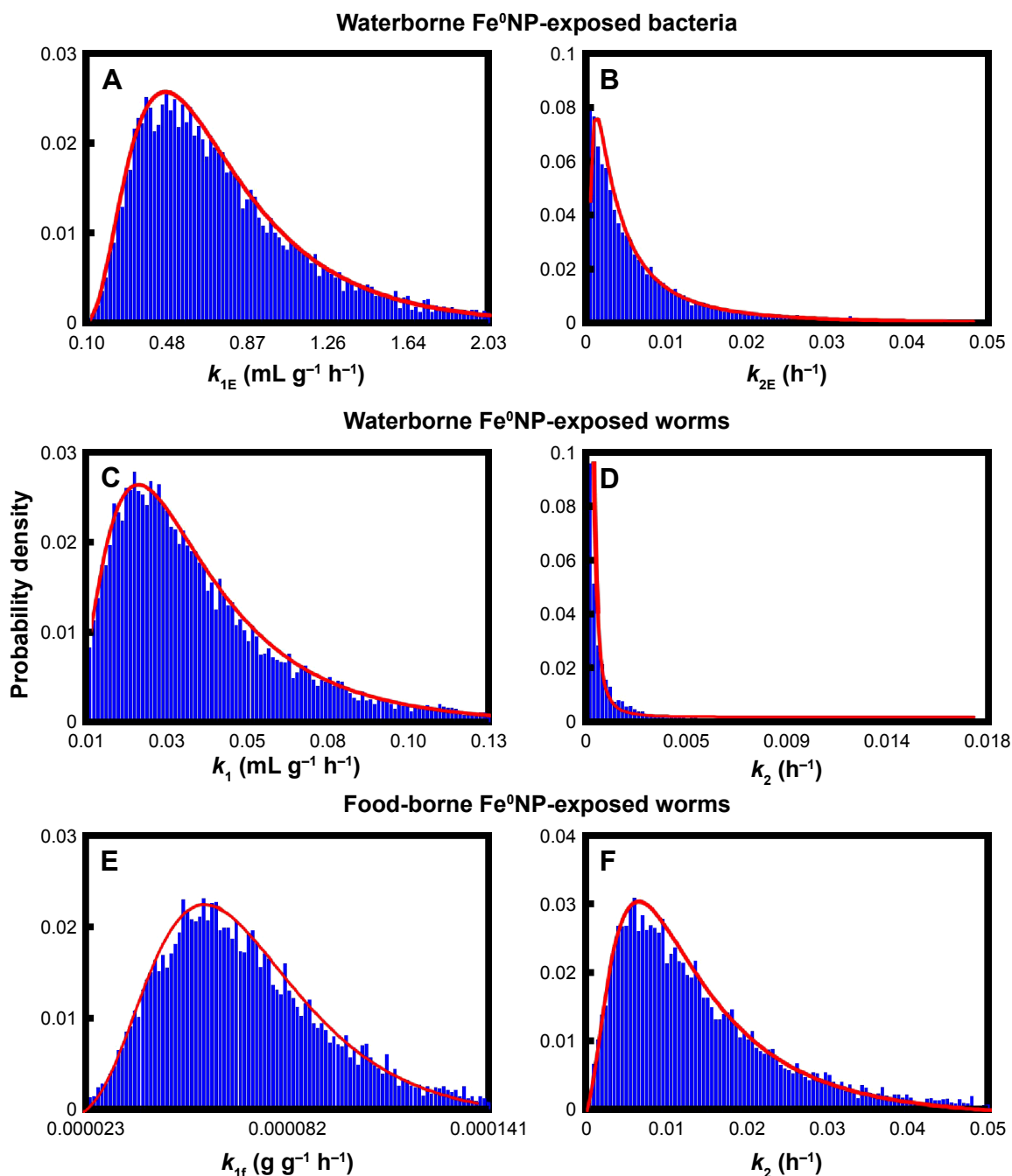
Figure 4 Probabilistic distributions.

Notes: Toxicokinetic parameter estimates of (**A**, **B**) uptake (k_{1E}) and elimination constants (k_{2E}) of waterborne Fe⁰NP-exposed *Escherichia coli* OP50, (**C**, **D**) uptake (k_1) and elimination constants (k_2) of waterborne Fe⁰NP-exposed *Caenorhabditis elegans*, and (**E**, **F**) uptake (k_{1f}) and elimination constants (k_{2f}) of food-borne Fe⁰NP-exposed *C. elegans*.
Abbreviations: NP, nanoparticle; f, food-borne; E, *E. coli* OP50; C, *C. elegans*.

significantly reduced by Fe⁰NP toxicity in higher concentrations of 500–10,000 mg·L⁻¹.[17]

Limitations and implications

We did not take physiological parameters (eg, assimilation efficiency, ingestion rate, or growth rate) into account in the TBTK modeling as in the previous studies.[37,75] However, it has been found that some of these physiological parameters do not have significant influence on sublethal endpoints, such as growth and reproduction, in worms.[75]

It has been suggested that variations in any TBTK data set could be associated with biological variation, experimental, and analytical errors.[76] To determine biomass of small organisms more rigorously, a previous study proposed
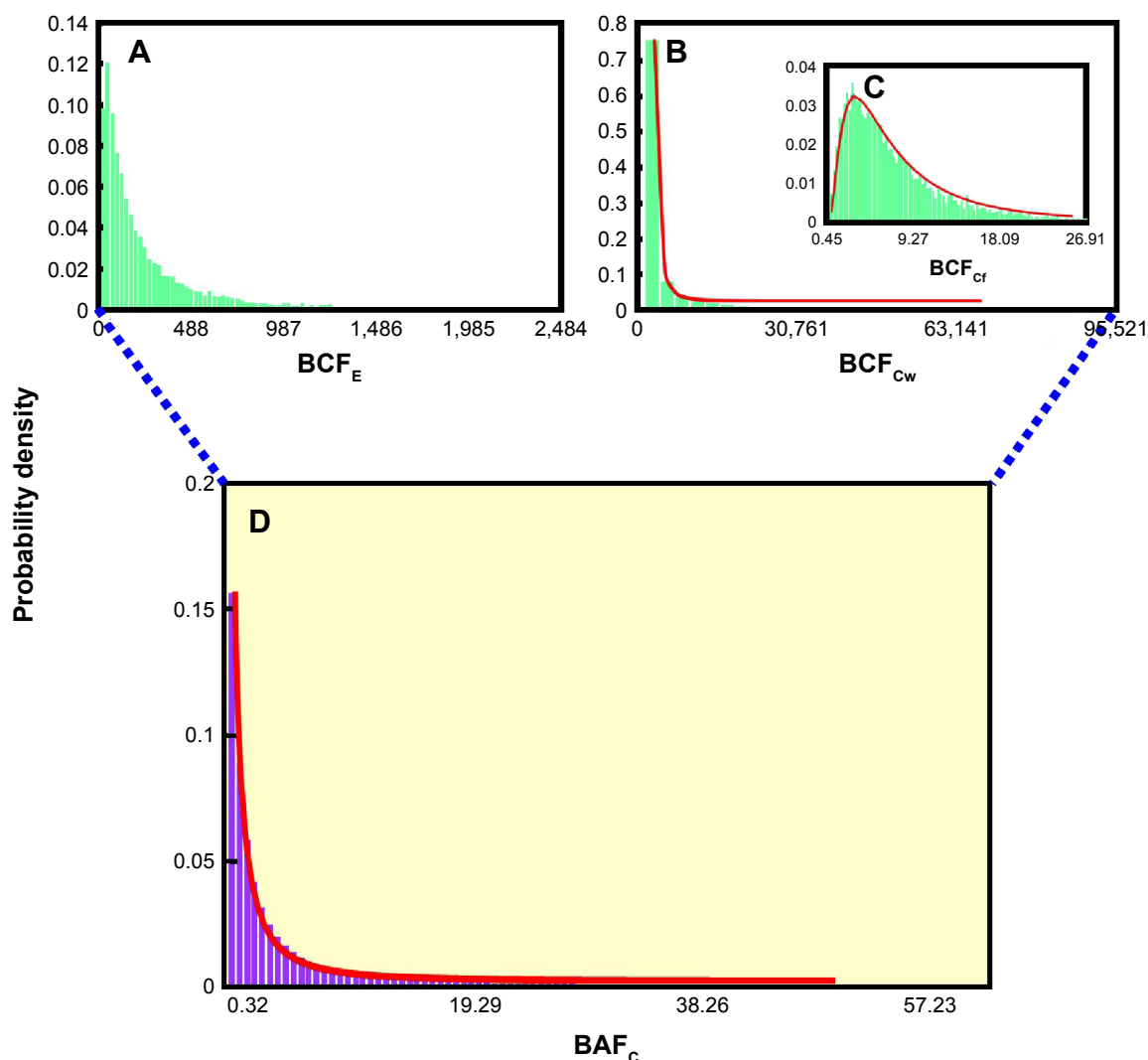
Figure 5 BCFs and BAF$_C$.
Notes: (**A**) Waterborne Fe^{0}NP-exposed *Escherichia coli* OP50; (**B**) waterborne Fe^{0}NP-exposed *Caenorhabditis elegans*; (**C**) food-borne Fe^{0}NP-exposed *C. elegans*; (**D**) bioaccumulation factor in *C. elegans* determined by probability density functions of BCF$_E$, BCF$_{Cw}$, and BCF$_{Cf}$.
Abbreviations: BCF, bioconcentration factor; BAF, bioaccumulation factor; E, *E. coli* OP50; C, *C. elegans*; w, waterborne; f, food-borne.

a method by using tissue-element contents as a proxy for biomass determination.[53] This method could be used as an alternative for quantification of Fe^{0}NP body burdens in the TBTK experiments. It was noted that the greatest variations were observed in the uptake phases in the TBTK experiments, suggesting that biological variations, such as chemical trafficking and detoxification, could be important determinants for individual body burdens.[76] It has been indicated that *C. elegans* has a labile iron pool for Fe metabolism in that cytosolic Fe was incorporated into Fe-containing proteins and transported to mitochondria for Fe-S biosynthesis.[77] Therefore, some undetectable Fe species could be attributable to biotransformation in *C. elegans*.

The TBTK/TD model can also link a bioenergetic-based model reflecting mode of action to simulate growth of *C. elegans* under different exposure scenarios. The well-established bioenergetic-toxicity model is based on the dynamic energy budget (DEB) theory, also known as the DEBtox model.[78] The DEBtox model describes modes of action of chemical toxicity based on the emphasis of resource allocation. DEBtox indicates that chemical effects act by way of three modes of action, including direct effects on growth and indirect effects on maintenance and food assimilation, and that only one of these effects occurs at a time in the lower effect range of the chemical.[78]

The life history and population growth of two *C. elegans* strains was compared and analyzed utilizing DEBtox modeling,[79] implying different reproductive strategies and physiological mechanisms. Another study used DEBtox modeling to explore the physiological mode of action of Cd,[80]
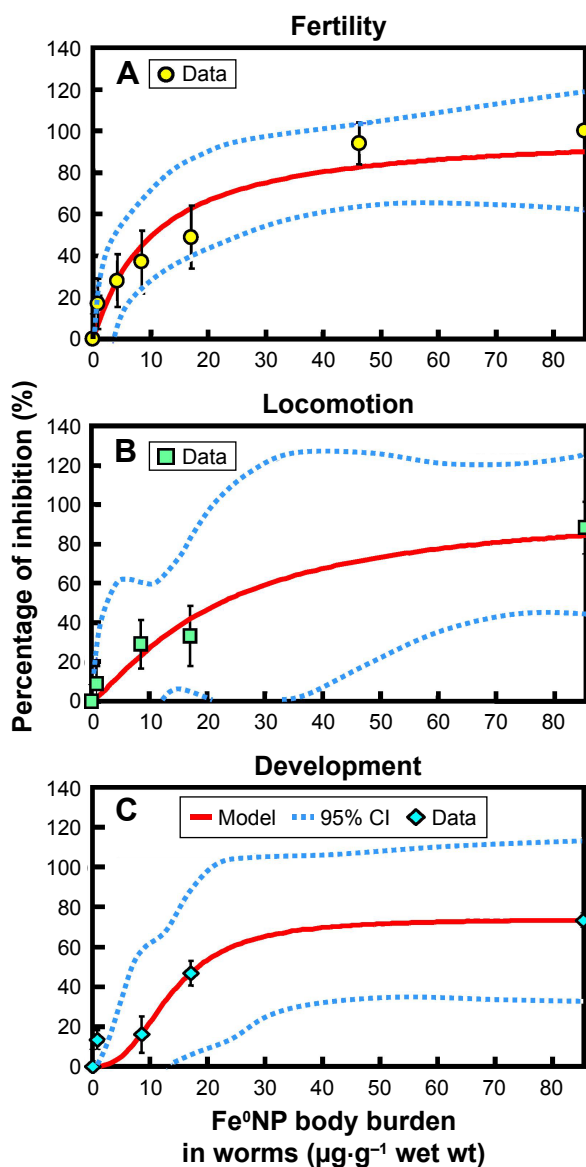
Figure 6 Reconstructed dose–response profiles.
Notes: Relationships between Fe⁰NP body burdens and inhibition of (**A**) fertility, (**B**) locomotion, and (**C**) development in *Caenorhabditis elegans*. Solid circles, squares, and diamonds are data points of concentration inhibition of fertility, locomotion, and development, respectively, in *C. elegans*. Solid and dotted lines are model simulations and 95% CIs, respectively.
Abbreviations: NP, nanoparticle; wt, weight.

suggesting that energy assimilation from food was the main factor dictating Cd toxicity. Mechanisms of action of aldicarb have been investigated using DEBtox modeling, revealing that an increase in energy demands was associated with maintenance in somatic and reproductive tissues.[81] It was found that uranium affected assimilation of energy from food and disrupted growth and reproduction in *C. elegans* based on the DEBtox model.[75]

Taken together, although there are plausible uncertainties in the experiments and the modeling, our toxicity bioassays and the TBTK/TD modeling in worms could be extensively

applied in environmental and health-risk analysis. By adopting exposure- and field-based information of Fe⁰NPs, the concentration–response relationships constructed in worms will make substantial progress in a quantitative risk assessment.

Conclusion

Our novel approach provides TBTK/TD-based empirical data on bioaccumulation and nanotoxicity of Fe⁰NPs in *C. elegans*. The TBTK/TD-based assessment model could greatly improve our ability to evaluate environmental and human health risks of Fe⁰NPs and to sustain ecohealth without overusing Fe⁰NPs for environmental remediation. We estimated that the average IC_{10} for fertility, locomotion, and development in *C. elegans* was 1.26, 3.84, and 6.78 µg·g⁻¹, respectively, which could also be used in future risk assessment. We conclude that *C. elegans* may be a superb in vivo model for specific nanotoxicity-property studies that provide adequate and rapid outcomes, giving insights into the understanding of the relationships between the physicochemical properties of nanomaterials and their toxicity. We conclude that the use of the TBTK/TD scheme manipulating *C. elegans* could be used for rapidly evaluating the in vivo toxicity of NPs or for drug screening in the field of nanomedicine. Finally, we suggest that TBTK/TD assessment for predicting NP-induced toxicity at different concentrations and conditions in *C. elegans* could enable rapid selection of nanomaterials that are more likely to be nontoxic in larger animals.

Author contributions

All authors contributed toward data analysis, drafting and critically revising the paper, and agree to be accountable for all aspects of the work.

Disclosure

The authors report no conflicts of interest in this work.

References
1. Wang CB, Zhang WX. Synthesizing nanoscale iron particles for rapid and complete dechlorination of TCE and PCBs. *Environ Sci Technol*. 1997;31(7):2154–2156.
2. Zhang X, Lin S, Chen Z, Megharaj M, Naidu R. Kaolinite-supported nanoscale zero-valent iron for removal of Pb²⁺ from aqueous solution: reactivity, characterization and mechanism. *Water Res*. 2011;45(1):3481–3488.

3. Fajardo C, Ortiz LT, Rodriguez-Membibre ML, Nande M, Lobo MC, Martin M. Assessing the impact of zero-valent iron (ZVI) nanotechnology on soil microbial structure and functionality: a molecular approach. *Chemosphere*. 2012;86(8):802–808.

4. Gomes HI, Dias-Ferreira C, Ribeiro AB. Overview of in situ and ex situ remediation technologies for PCB-contaminated soils and sediments and obstacles for full-scale application. *Sci Total Environ*. 2013; 445–446:237–260.

5. Gil-Díaz MM, Pérez-Sanz A, Vicente MÁ, Lobo MC. Immobilisation of Pb and Zn in soils using stabilised zero-valent iron nanoparticles: effects on soil properties. *Clean Soil Air Water*. 2014;42(12):1776–1784.

6. Němeček J, Lhotský O, Cajthaml T. Nanoscale zero-valent iron application for in situ reduction of hexavalent chromium and its effects on indigenous microorganism populations. *Sci Total Environ*. 2014;485–486:739–747.

7. Auffan M, Achouak W, Rose J, et al. Relation between the redox state of iron-based nanoparticles and their cytotoxicity toward *Escherichia coli*. *Environ Sci Technol*. 2008;42(17):6730–6735.

8. Keenan CR, Goth-Goldstein R, Lucas D, Sedlak DL. Oxidative stress induced by zero-valent iron nanoparticles and Fe(II) in human bronchial epithelial cells. *Environ Sci Technol*. 2009;43(12):4555–4560.

9. Barnes RJ, van der Gast CJ, Riba O, et al. The impact of zero-valent iron nanoparticles on a river water bacterial community. *J Hazard Mater*. 2010;184(1–3):73–80.

10. Chen PJ, Tan SW, Wu WL. Stabilization or oxidation of nanoscale zerovalent iron at environmentally relevant exposure changes bioavailability and toxicity in medaka fish. *Environ Sci Technol*. 2012;46(15): 8431–8439.

11. El-Temsah YS, Joner EJ. Ecotoxicological effects on earthworms of fresh and aged nano-sized zero-valent iron (nZVI) in soil. *Chemosphere*. 2012;89(1):76–82.

12. Kadar E, Rooks P, Lakey C, White DA. The effect of engineered iron nanoparticles on growth and metabolic status of marine microalgae cultures. *Sci Total Environ*. 2012;439:8–17.

13. Keller AA, Garner K, Miller RJ, Lenihan HS. Toxicity of nano-zero valent iron to freshwater and marine organisms. *PLoS One*. 2012; 7(8):e43983.

14. Chen PJ, Wu WL, Wu KC. The zerovalent iron nanoparticle causes higher developmental toxicity than its oxidation products in early life stages of medaka fish. *Water Res*. 2013;47(12):3899–3909.

15. Ma X, Gurung A, Deng Y. Phytotoxicity and uptake of nanoscale zero-valent iron (nZVI) by two plant species. *Sci Total Environ*. 2013; 443:844–849.

16. Pawlett M, Ritz K, Dorey RA, Rocks S, Ramsden J, Harris JA. The impact of zero-valent iron nanoparticles upon soil microbial communities is context dependent. *Environ Sci Pollut Res Int*. 2013;20(2):1041–1049.

17. Saccà ML, Fajardo C, Costa G, Lobo C, Nande M, Martin M. Integrating classical and molecular approaches to evaluate the impact of nano-sized zero-valent iron (nZVI) on soil organisms. *Chemosphere*. 2014; 104:184–189.

18. Otero-González L, Sierra-Alvarez R, Boitano S, Field JA. Application and validation of an impedance-based real time cell analyzer to measure the toxicity of nanoparticles impacting human bronchial epithelial cells. *Environ Sci Technol*. 2012;46(18):10271–10278.

19. Sun Z, Yang L, Chen KF, et al. Nano zerovalent iron particles induce pulmonary and cardiovascular toxicity in an in vitro human co-culture model. *Nanotoxicology*. 2016;10(7):881–890.

20. Lee C, Kim JY, Lee WI, Nelson KL, Yoon J, Sedlak DL. Bactericidal effect of zero-valent iron nanoparticles on *Escherichia coli*. *Environ Sci Technol*. 2008;42(13):4927–4933.

21. Li H, Zhou Q, Wu Y, Fu J, Wang T, Jiang G. Effects of waterborne nano-iron on medaka (*Oryzias latipes*): antioxidant enzymatic activity, lipid peroxidation and histopathology. *Ecotoxicol Environ Saf*. 2009; 72(3):684–692.

22. Chaithawiwat K, Vangnai A, McEvoy JM, Pruess B, Krajangpan S, Khan E. Role of oxidative stress in inactivation of *Escherichia coli* BW25113 by nanoscale zero-valent iron. *Sci Total Environ*. 2016;565: 857–862.

23. Lei C, Zhang L, Yang K, Zhu L, Lin D. Toxicity of iron-based nanoparticles to green algae: effects of particle size, crystal phase, oxidation state and environmental aging. *Environ Pollut*. 2016;218:505–512.

24. Libralato G, Devoti AC, Zanella M, et al. Phytotoxicity of ionic, micro- and nano-sized iron in three plant species. *Ecotoxicol Environ Saf*. 2016; 123:81–88.

25. Yirsaw BD, Mayilswami S, Megharaj M, et al. Effect of zero valent iron nanoparticles to *Eisenia fetida* in three soil types. *Environ Sci Pollut Res Int*. 2016;23(10):9822–9831.

26. Chou BYH, Liao CM, Lin MC, Cheng HH. Toxicokinetics/toxicodynamics of arsenic for farmed juvenile milkfish *Chanos chanos* and human consumption risk in BFD-endemic area of Taiwan. *Environ Int*. 2006;32(4):545–553.

27. Tsai JW, Chen WY, Ju YR, Liao CM. Bioavailability links mode of action can improve the long-term field risk assessment for tilapia exposed to arsenic. *Environ Int*. 2009;35(4):727–736.

28. Ashauer R, Escher BI. Advantages of toxicokinetic and toxicodynamic modelling in aquatic ecotoxicology and risk assessment. *J Environ Monit*. 2010;12(11):2056–2061.

29. Chen WY, Cheng YH, Hsieh NH, et al. Physiologically based pharmacokinetic modeling of zinc oxide nanoparticles and zinc nitrate in mice. *Int J Nanomedicine*. 2015;10:6277–6292.

30. Valencia PM, Farokhzad OC, Karnik R, Langer R. Microfluidic technologies for accelerating the clinical translation of nanoparticles. *Nat Nanotechnol*. 2012;7(10):623–629.

31. Freeman MN, Peredney CL, Williams PL. A soil bioassay using the nematode *Caenorhabditis elegans*. In: Henshel DS, Black MC, Harrass MC, editors. *Environmental Toxicology and Risk Assessment: Standardization of Biomarkers for Endocrine Disruption and Environmental Assessment*. West Conshohocken (PA): American Society for Testing and Materials; 2000:305–318.

32. Peredney CL, Williams PL. Utility of *Caenorhabditis elegans* for assessing heavy metal contamination in artificial soil. *Arch Environ Contam Toxicol*. 2000;39(1):113–118.

33. Roh JY, Sim SJ, Yi J, et al. Ecotoxicity of silver nanoparticles on the soil nematode *Caenorhabditis elegans* using functional ecotoxicogenomics. *Environ Sci Technol*. 2009;43(10):3933–3940.

34. Sakaue Y, Kim J, Miyamoto Y. Effects of TAT-conjugated platinum nanoparticles on lifespan of mitochondrial electron transport complex I-deficient *Caenorhabditis elegans, nuo-1. Int J Nanomedicine*. 2010;5: 687–695.

35. Charão MF, Souto C, Brucker N, et al. *Caenorhabditis elegans* as an alternative in vivo model to determine oral uptake, nanotoxicity, and efficacy of melatonin-loaded lipid-core nanocapsules on paraquat damage. *Int J Nanomedicine*. 2015;10:5093–5106.

36. Jager T, Gudmundsdóttir EM, Cedergreen N. Dynamic modeling of sublethal mixture toxicity in the nematode *Caenorhabditis elegans*. *Environ Sci Technol*. 2014;48(12):7026–7033.

37. Spann N, Goedkoop W, Traunspurger W. Phenanthrene bioaccumulation in the nematode *Caenorhabditis elegans*. *Environ Sci Technol*. 2015; 49(3):1842–1850.

38. Margerit A, Gomez E, Gilbin R. Dynamic energy-based modeling of uranium and cadmium joint toxicity to *Caenorhabditis elegans*. *Chemosphere*. 2016;146:405–412.

39. He F, Zhao D. Manipulating the size and dispersibility of zerovalent iron nanoparticles by use of carboxymethyl cellulose stabilizers. *Environ Sci Technol*. 2007;41(17):6216–6221.

40. Andrássy I. Rauminhalts und gewichtsbestimmung der fadenwürmer (nematoden). *Acta Zool*. 1956;2:1–15.

41. Haitzer M, Höss S, Traunspurger W, Steinberg C. Effects of dissolved organic matter (DOM) on the bioconcentration of organic chemicals in aquatic organisms: a review. *Chemosphere*. 1998;37(7): 1335–1362.

42. Yang YF, Chen PJ, Liao VH. Nanoscale zerovalent iron (nZVI) at environmentally relevant concentrations induced multigenerational reproductive toxicity in *Caenorhabditis elegans*. *Chemosphere*. 2016; 150:615–623.

43. Boyd WA, McBride SJ, Rice JR, Snyder SW, Freedman JH. A high-throughput method for assessing chemical toxicity using a *Caenorhabditis elegans* reproduction assay. *Toxicol Appl Pharmacol*. 2010;245(2):153–159.

44. Tsalik EL, Hobert O. Functional mapping of neurons that control locomotory behavior in *Caenorhabditis elegans*. *J Neurobiol*. 2003;56(2): 178–197.

45. Stookey L. Ferrozine-a new spectrophotometric reagent for iron. *Anal Chem*. 1970;42(7):779–781.

46. Bourne DW. *Mathematical Modeling of Pharmacokinetic Data*. Chicago: Technomic; 1995.

47. Kirschling TL, Gregory KB, Minkley EG, Lowry GV, Tilton RD. Impact of nanoscale zero valent iron on geochemistry and microbial populations in trichloroethylene contaminated aquifer materials. *Environ Sci Technol*. 2010;44(9):3474–3480.

48. Miyamoto A, Tokumoto H, Konishi Y, Nomura T. Ecotoxicity of PSL nanoparticles to *Escherichia coli*. *J Soc Powder Technol*. 2012;49(5):362–366.

49. Kumar A, Pandey AK, Singh SS, Shanker R, Dhawan A. Cellular uptake and mutagenic potential of metal oxide nanoparticles in bacterial cells. *Chemosphere*. 2011;83(8):1124–1132.

50. Yan D, Yin G, Huang Z, et al. Cellular compatibility of biomineralized ZnO nanoparticles based on prokaryotic and eukaryotic systems. *Langmuir*. 2011;27(21):13206–13211.

51. Li Y, Zhang W, Niu J, Chen Y. Mechanism of photogenerated reactive oxygen species and correlation with the antibacterial properties of engineered metal-oxide nanoparticles. *ACS Nano*. 2012;6(6):5164–5173.

52. Djurišić AB, Leung YH, Ng AM, et al. Toxicity of metal oxide nanoparticles: mechanisms, characterization, and avoiding experimental artefacts. *Small*. 2015;11(1):26–44.

53. Verschoor MJ, Molot LA. A comparison of three colorimetric methods of ferrous and total reactive iron measurement in freshwaters. *Limnol Oceanogr Methods*. 2013;11(3):113–125.

54. Crommentuijn T, Doodeman CJ, Doornekamp A, van der Pol JJ, van Gestel CA, Bedaux JJ. Lethal body concentrations and accumulation patterns determine time-dependent toxicity of cadmium in soil arthropods. *Environ Toxicol Chem*. 1994;13(11):1781–1789.

55. Díez-Ortiz M, Giska I, Groot M, Borgman EM, van Gestel CA. Influence of soil properties on molybdenum uptake and elimination kinetics in the earthworm. *Chemosphere*. 2010;80(9):1036–1043.

56. Allen HE, Hall RH, Brisbin TD. Metal speciation: effects on aquatic toxicity. *Environ Sci Technol*. 1980;14(4):441–443.

57. Chapman PM, Allen HE, Godtfredsen K, Z'graggen MN. Evaluation of bioaccumulation factors in regulating metals. *Environ Sci Technol*. 1996;30(10):448A–452A.

58. Offermann K, Matthäi A, Ahlf W. Assessing the importance of diet-borne cadmium and particle characteristics on bioavailability and bioaccumulation in the nematode *Caenorhabditis elegans*. *Environ Toxicol Chem*. 2009;28(6):1149–1158.

59. Tourinho PS, van Gestel CA, Morgan AJ, et al. Toxicokinetics of Ag in the terrestrial isopod *Porcellionides pruinosus* exposed to Ag NPs and AgNO₃ via soil and food. *Ecotoxicology*. 2016;25(2):267–278.

60. Judy JD, Unrine JM, Bertsch PM. Evidence for biomagnification of gold nanoparticles within a terrestrial food chain. *Environ Sci Technol*. 2011;45(2):776–781.

61. Majumdar S, Trujillo-Reyes J, Hernandez-Viezcas JA, et al. Cerium biomagnification in a terrestrial food chain: influence of particle size and growth stage. *Environ Sci Technol*. 2016;50(13):6782–6792.

62. Chen J, Li H, Han X, et al. Transmission and accumulation of nano-TiO₂ in a 2-step food chain (*Scenedesmus obliquus* to *Daphnia magna*). *Bull Environ Contam Toxicol*. 2015;95:145–149.

63. Werlin R, Priester JH, Mielke RE, et al. Biomagnification of cadmium selenide quantum dots in a simple experimental microbial food chain. *Nat Nanotechnol*. 2011;6(1):65–71.

64. Lewinski NA, Zhu H, Ouyang CR, et al. Trophic transfer of amphiphilic polymer coated CdSe/ZnS quantum dots to *Danio rerio*. *Nanoscale*. 2011;3(8):3080–3083.

65. Mielke RE, Priester JH, Werlin RA, et al. Differential growth of and nanoscale TiO₂ accumulation in *Tetrahymena thermophila* by direct feeding versus trophic transfer from *Pseudomonas aeruginosa*. *Appl Environ Microbiol*. 2013;79(18):5616–5624.

66. Yooiam M, Chaichana R, Satapanajaru T. Toxicity, bioaccumulation and biomagnification of silver nanoparticles in green algae (*Chlorella* sp.), water flea (*Moina macrocopa*), blood worm (*Chironomus* spp.) and silver barb (*Barbonymus gonionotus*). *Chem Spec Bioavailab*. 2014;26(4): 257–265.

67. Zhu X, Wang J, Zhang X, et al. Trophic transfer of TiO₂ nanoparticles from *Daphnia* to zebrafish in a simplified freshwater food chain. *Chemosphere*. 2010;79(9):928–933.

68. Tangaa SR, Selck H, Winther-Nielsen M, Khan FR. Trophic transfer of metal-based nanoparticles in aquatic environments: a review and recommendations for future research focus. *Environ Sci Nano*. 2016;3: 966–981.

69. Unrine JM, Shoults-Wilson WA, Zhurbich O, et al. Trophic transfer of Au nanoparticles from soil along a simulated terrestrial food chain. *Environ Sci Technol*. 2012;46(17):9753–9760.

70. Yu ZY, Zhang J, Yin DQ. Toxic and recovery effects of copper on *Caenorhabditis elegans* by various food-borne and water-borne pathways. *Chemosphere*. 2010;87(11):1361–1367.

71. Mitchell DH, Stiles JW, Santelli J, Sanadi DR. Synchronous growth and aging of *Caenorhabditis elegans* in the presence of fluorodeoxyuridine. *J Gerontol*. 1979;34(1):28–36.

72. Gandhi S, Santelli J, Mitchell DH, Stiles JW, Sanadi DR. A simple method for maintaining large, aging populations of *Caenorhabditis elegans*. *Mech Ageing Dev*. 1980;12(2):137–150.

73. Zuckerman BM. Achievement of age synchrony in *Caenorhabditis elegans*. *J Gerontol*. 1980;35(2):282–283.

74. Gruber J, Ng LF, Poovathingal SK, Halliwell B. Deceptively simple but simply deceptive – *Caenorhabditis elegans* lifespan studies: considerations for aging and antioxidant effects. *FEBS Lett*. 2009;583(21): 3377–3387.

75. Goussen B, Beaudouin R, Dutilleul M, Buisset-Goussen A, Bonzom JM, Pery AR. Energy-based modelling to assess effects of chemicals on *Caenorhabditis elegans*: a case study on uranium. *Chemosphere*. 2015; 120:507–514.

76. Spurgeon DJ, Lister L, Kille P, Pereira MG, Wright J, Svendsen C. Toxicokinetic studies reveal variability in earthworm pollutant handling. *Pedobiologia*. 2011;54 Suppl:S217–S222.

77. Anderson CP, Leibold EA. Mechanisms of iron metabolism in *Caenorhabditis elegans*. *Front Pharmacol*. 2014;5:113.

78. Kooijman SA, Bedaux JJ. *The Analysis of Aquatic Toxicity Data*. Amsterdam: VU University Press; 1996.

79. Alda Alvarez O, Jager T, Redondo EM, Kammenga JE. Physiological modes of action of toxic chemicals in the nematode *Acrobeloides nanus*. *Environ Toxicol Chem*. 2006;25(12):3230–3237.

80. Swain S, Wren JF, Stürzenbaum SR, et al. Linking toxicant physiological mode of action with induced gene expression changes in *Caenorhabditis elegans*. *BMC Syst Biol*. 2010;4:32.

81. Wren JF, Kille P, Spurgeon DJ, Swain S, Sturzenbaum SR, Jager T. Application of physiologically based modelling and transcriptomics to probe the systems toxicology of aldicarb for *Caenorhabditis elegans* (Maupas 1900). *Ecotoxicology*. 2011;20(2):397–408.

Supplementary materials

Table S1 Experimental data (mean ± SD) of toxic effects (%) of Fe⁰NPs on *Caenorhabditis elegans*

Nominal concentrations of Fe⁰NPs (mg·L⁻¹)						
0	**5**	**25**	**50**	**100**	**250**	**500**
Inhibition of fertility						
0±12.26	16.9±0.12	27.93±12.57	37.14±15.08	49.36±15.09	93.66±10.27	100±0
Inhibition of locomotion						
0±8.66	13.53±4.79	–	16.09±9.12	46.8±6.27	–	73.37±3.68
Inhibition of development						
0±8.61	9.1±9.44	–	29±15.14	33.2±13.16	–	88.3±6.36

Note: "–" Data unavailable.
Abbreviations: SD, standard deviation; NPs, nanoparticles.

Table S2 Bioconcentration potency in the bacteria *Escherichia coli* OP50

Nominal concentration of total iron in dosing solution (mg·L⁻¹)	Iron concentration in *E. coli* OP50[a] (µg·g⁻¹)	BCF[b] (L·kg⁻¹)
0	697.42±295.01	–
5	764.5±253.85	152.92±50.86
25	1,324.5±55.86	52.98±2.23
100	2,167.95±1,445.84	21.68±14.46
500	11,118.743±11,458.645	22.24±22.91

Notes: [a]Data presented as mean ± SD (three replicates per concentration); [b]iron concentration in bacteria/total iron concentration of the dosing solution. Iron concentration measured by ferrozine method. "–" Data unavailable.
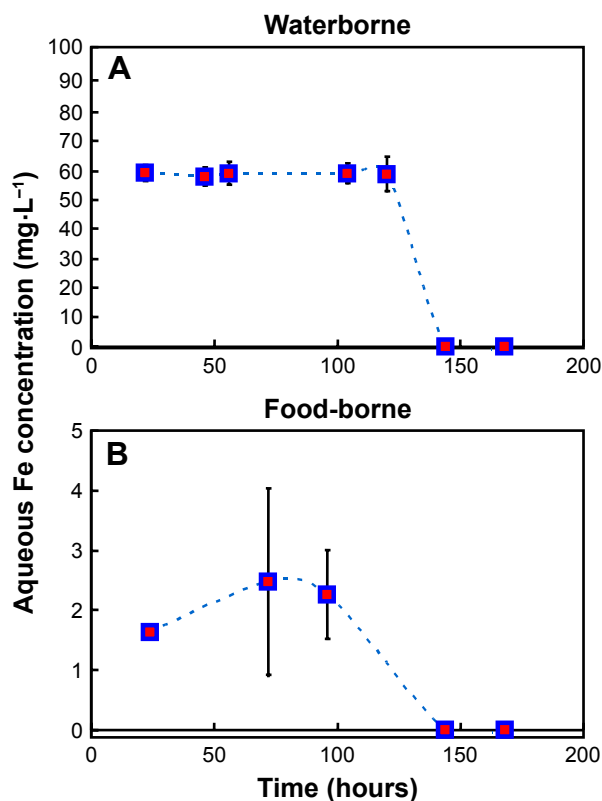**Abbreviations:** BCF, bioconcentration factor; SD, standard deviation.

Figure S1 Aqueous Fe concentrations over time for (**A**) waterborne and (**B**) food-borne exposure experiments.
Note: Dashed lines indicate the aqueous Fe concentration trend over time.

Table S3 Fitted coefficients (mean ± SE) of three-parameter Hill model describing the relationships between inhibition of fertility, locomotion, and development (%) and Fe^0NP concentrations ($mg \cdot L^{-1}$) in *Caenorhabditis elegans*

Fitted coefficient	Inhibition of fertility	Inhibition of locomotion	Inhibition of development
I_{max}	100±27.13*	100±47.05	74.09±10.33*
IC_{50}	10.39±7.49	22.28±24.22	13.89±3.02*
n	1.04±0.6	1.25±1.09	2.59±1.42
r^2	0.93	0.96	0.95
P-value	**	*	0.05

Notes: *$P<0.05$; **$P<0.01$.
Abbreviations: SE, standard error; NP, nanoparticle.